

# ACTIVE-PASSIVE HYBRID CONTROL OF SHOCK BUFFET

Chuanqiang Gao<sup>1</sup>, Kai Ren<sup>1</sup>, Weiwei Zhang<sup>1</sup>

<sup>1</sup> School of Aeronautics, Northwestern Polytechnical University, Xi'an, China, 710072

### **Abstract**

Shock buffet is a significant self-excited shock vibration phenomenon induced by shock wave boundary-layer interaction. For a swept wing, the unsteadiness contains the chordwise oscillation as well as the spanwise fluctuation of the shock, displaying the wideband and multimodal characteristics. Independent active or passive control can only reduce the amplitude of buffet load, while significant pressure fluctuations still persist. An active-passive cooperative control (APCC) scheme, which combines shock control bump (SCB) and trailing edge flap, is proposed to eliminate the oscillating loads of shock buffet. SCB is long in chordwise direction but narrow in spanwise direction, while its height remains small, which basically doesn't affect lift-drag ratio of wing, and can eliminate spanwise fluctuation of shock wave. The role of trailing edge flap is the same as that of 2D shock buffet active control, and it's used to eliminate chordwise oscillation of shock wave. The simulation results show that APCC can basically eliminates the pressure fluctuations on wing.

**Keywords:** shock buffet, active control, passive control

#### 1. Introduction

Transonic flight offers a balance between flight speed and energy consumption, so the civil aircraft use transonic flight as their cruising state. However, in transonic state, phenomena such as shock wave and shock wave-boundary layer interaction can result in various complex aerodynamic problems, affecting the aircraft's operational envelope. One prominent problem is shock buffet, also known as transonic buffet, which manifests as self-sustained oscillations of shock wave and periodic fluctuations in lift. This phenomenon can impact flight controllability, passenger comfort, and even lead to structural fatigue and flight accidents. Therefore, the effective control of shock buffet is a challenging and hot topic in the field of aviation[1–3].

Most transonic aircraft utilize swept wings because they can increase the drag divergence Mach number, weaken the shock wave intensity, and prevent severe stall of the wing. However, more complex three-dimensional shock buffet flow will occur on the swept wing. In addition to the forward and backward oscillation similar to two-dimensional problem in streamwise cross-section, shock wave also exhibits spanwise fluctuation, resulting in different phases of shock motion on each streamwise cross-section. Gao et al.[4]analyzed the characteristics of three-dimensional shock buffet flow using the Dynamic Mode Decomposition (DMD) method. The mode contours revealed that, in addition to the chordwise instability mode observed in two-dimensional flow, the 3D shock buffet flow also experiences spanwise instability due to the effects of aspect ratio and sweep angle, exhibiting more complex features. In terms of frequency, unlike the harmonic characteristics observed in the load spectrum of shock buffet for two-dimensional airfoils[5], three-dimensional swept-wing shock buffet exhibits a broader frequency characteristic[6].

Based on the above understanding of shock buffet flow, numerous control schemes have been employed to mitigate or eliminate self-sustained oscillation of shock wave. The main idea is to change the boundary layer or the shape of trailing edge to intervene the shock wave-boundary layer interaction zone and the flow at trailing edge. In the context of airfoils, various control techniques have been investigated, such as shock control bumps (SCB)[7], streamwise slots[8], vortex generators[\*], plasma actuators[10], trailing edge flaps[11], and other control surfaces[12].

There is also some research on shock buffet control of three-dimensional wings. The most commonly

employed approach is a passive control scheme based on shock control bumps. Mayer et al. [13, 14] compared the control effectiveness of two-dimensional bump and three-dimensional bump array for the AVERT (Aerodynamic Validation of Emission Reducing Technologies) wing. The results showed that the three-dimensional bump array can generate streamwise vortices, acting as vortex generators, which alleviates shock-induced separation. Molton et al.[15]utilized fluidic vortex generators (FVG) to suppress shock-induced separation and delay the onset of shock buffet. This method avoids the disadvantage of mechanical vortex generators, which increase drag during cruising conditions, but it requires a continuous energy supply. Dandois et al.[16] further applied FVG into closed-loop control system, and although the shock buffet was not eliminated completely, the amplitude of pressure fluctuation on the wing surface was reduced.

The current research results indicate that for two-dimensional shock buffet dominated by shock wave chordwise oscillation, shock control bumps or trailing edge flaps can completely suppress shock wave oscillation. Moreover, closed-loop control based on trailing edge flap can even maintain the lift-to-drag ratio and other aerodynamic performance of the airfoil. However, for more complex three-dimensional shock buffet flow on wings, there are both chordwise oscillation and spanwise fluctuation of shock wave, current control efforts are primarily focused on passive control, with limited research on active control. This is because active control systems are complex and inappropriate active control strategies for high-dimensional nonlinear shock buffet flow of wings may be less effective than simple and efficient passive control. Furthermore, current control schemes for shock buffet of wings cannot completely eliminate fluctuating loads and usually rely on single control mechanism. Therefore, considering the characteristic of spanwise fluctuation and chordwise oscillation of shock wave exhibited in three-dimensional shock buffet flow, this study aims to explore the use of an active-passive cooperative control method to control three-dimensional shock buffet flow, thereby enhance flow stability.

## 2. Numerical Simulation Method

In terms of three-dimensional shock buffet numerical simulation, due to limitations in computational cost, current research mainly focuses on unsteady Reynolds-averaged Navier-Stokes simulation, with a small amount of Detached Eddy Simulation (DES) simulation. For shock buffet flow dominated by shock wave oscillation, although DES provides a more refined simulation of flow, the main characteristics of the flow are generally consistent with URANS results.

The SST k-w turbulence model is introduced to close the Reynolds-averaged equation, and the spatial discretization and time integration of turbulent and mean flows are carried out in a loosely coupled way. The second-order advection upstream splitting method (AUSM)+ scheme is conducted to evaluate the inviscid flux with a reconstruction technique. The viscous flux term is discretized by the standard central scheme. In the turbulence model, the convective term is discretized by the second-order AUSM scheme and the destruction term by the second-order central scheme. For the simulation of unsteady flow, the dual time stepping method is used to solve the governing equations. At the subiteration, the fourth order Runge-Kutta scheme is used with a local time stepping.

CRM wing-body model is selected to verify the simulation.

This study first compares the pressure distribution of the steady flow field. At M=0:847, a=2:47deg., and Re = 2:2x10<sup>6</sup>, the pressure distribution on the surface of CRM model is shown in Fig. 1, while Fig. 2 shows the comparison between the calculated pressure coefficient distribution on the typical cross-section and the experimental results[17]. The numerical simulation results are basically consistent with the experimental results, although the predicted shock wave position is slightly downstream compared to the experiment. This is consistent with Ohmichi's conclusion[18], and it may be attributed to the unmodified incoming angle of attack in our calculations. Overall, the URANS simulation in this study have been able to predict the shock and its separation characteristics on the wing with reasonable accuracy.

In the simulation of buffet load, at M= 0:85, a= 4:9deg, Re =2.2x10<sup>6</sup>, this study compares the RMS (root mean square) distribution of pressure coefficients on wing surface, as shown in Fig. 3. The larger RMS values indicate more severe pressure fluctuations. The dark region at the leading edge represents the region of shock wave oscillation, while the lighter region at the trailing edge represents the separation zone after the shock wave. It can be seen that the URANS method utilized in this study successfully captures the dynamic characteristics caused by shock wave oscillation, and the range of significant shock wave oscillation is in good agreement with experimental result [19].

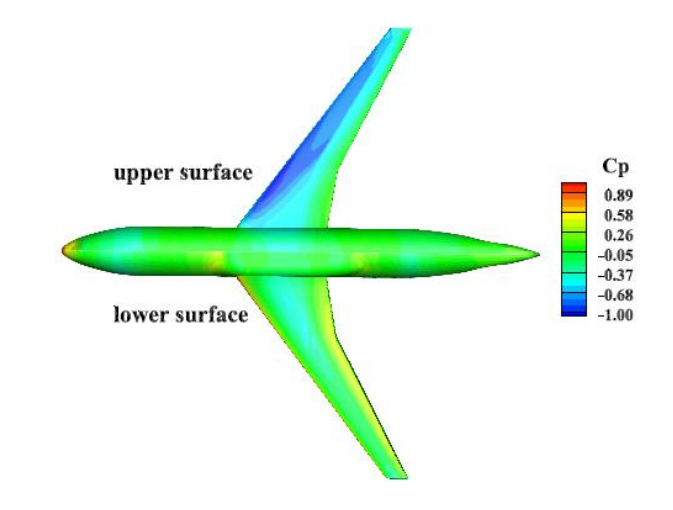


Figure 1 Calculated surface pressure distribution of CRM model.

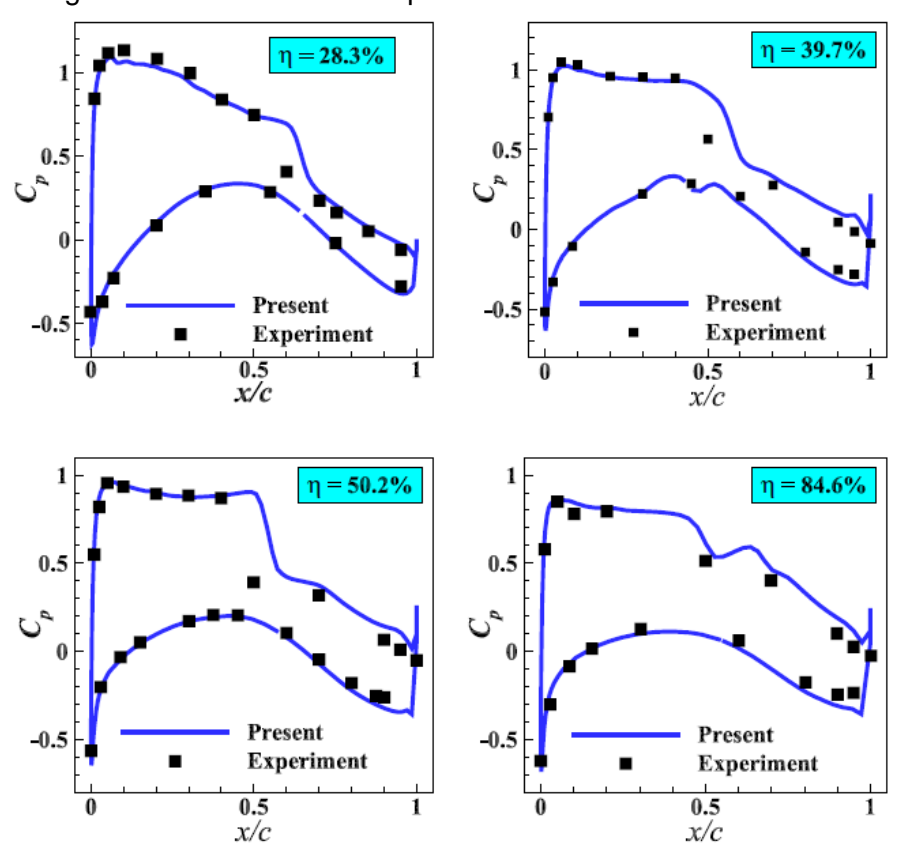


Figure 2 Comparison of pressure coefficient of typical cross-section with experimental results.

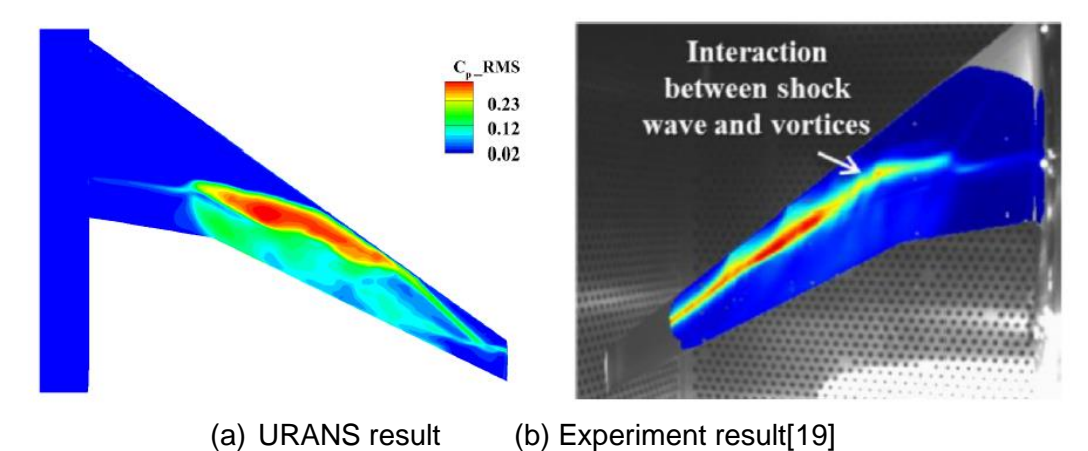


Figure 3 Distribution of RMS of pressure coefficient on upper surface of CRM.

# 3. Active-passive Cooperative Control Scheme

In this study, the research object gradually transitions from a small aspect ratio wing section to a large aspect ratio swept wing, and the spanwise fluctuation characteristics in shock buffet flow will gradually become significant. To address the chordwise oscillation and spanwise fluctuation characteristics of shock buffet flow for three-dimensional wings, this study proposes the following active-passive cooperative control scheme, as shown in Fig. 4. The passive control method is shock control bump. Drawing on the design idea of wing fences, the SCB with a smaller spanwise width and a longer chordwise length are employed to suppress spanwise fluctuation of shock wave. As for active control, the actuator is trailing edge flap, similar to the control scheme for shock buffet of two-dimensional airfoil. By designing the feedback control signal, the deflection of flap is utilized to suppress the chordwise oscillation of the shock wave. The following sections provide an introduction to the design for active control and passive control, respectively.

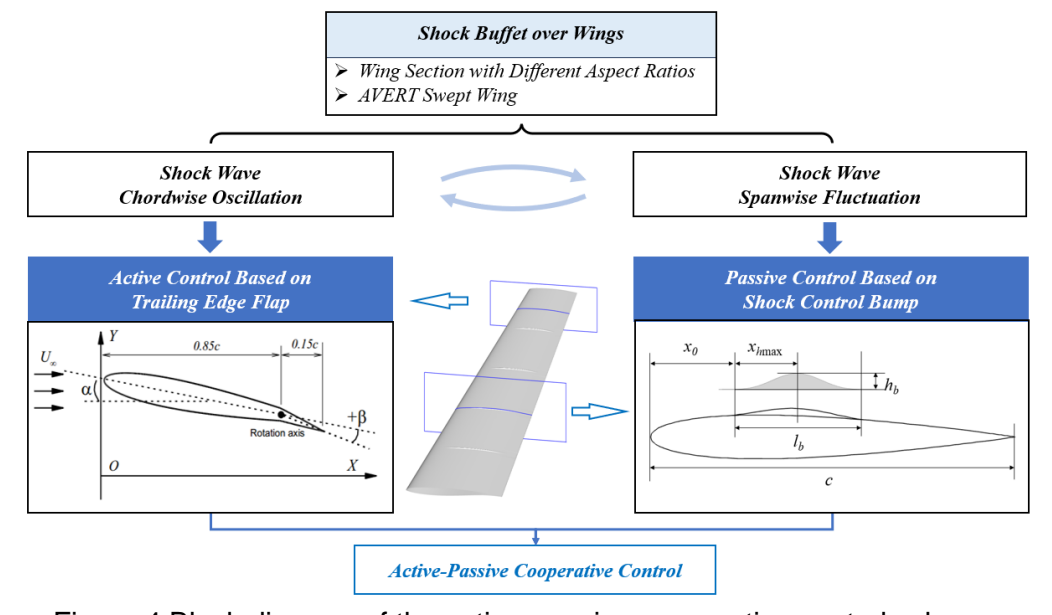


Figure 4 Block diagram of the active-passive cooperative control scheme.

(1)

# 4. Shock Buffet Control for AVERT Wing

AVERT wing is used in the Aerodynamic Validation of Emission Reducing Technologies project launched by ONERA in 2007, and a series of shock buffet control studies have been carried out based on this wing. AVERT wing is based on the supercritical OAT15A airfoil, the sweep angle at leading edge is 30 degrees, the span length L=1:225m, the chord length at wing root is 0.450m, and the chord length at wing tip is 0.225m. Dandois[20] used the RMS of lift coefficient and pressure coefficient at the trailing edge as the criterion of the onset boundary of shock buffet in the experiment, and observed that the onset angle of shock buffet was about 3 degrees at  $Re=2.83\times10^6$  and Mach number

M = 0.82.

## 4.1 Characteristic Analysis of Shock Buffet Flow on AVERT Wing

At M = 0.82,  $\alpha = 3.58$  deg.,  $Re=2:83\times10^6$ , for the shock buffet flow of AVERT wing, the RMS distribution of pressure on wing surface is shown in Fig. 5. The pressure pulsation exists from wing root to wing tip, and is more significant in the wing tip region. This is consistent with the phenomenon observed by references, when the angle of attack is close to the buffet onset boundary, the shock wave at the wing tip region become unstable first, resulting in the largest magnitude of pressure pulsation. Select sampling points S1 and S2 on the upper surface of the wing with different spanwise sections. The time histories of pressure coefficient at these sampling points are shown in Fig. 6. It can be seen that the pulsation frequency at different sampling points is basically the same, but the phase is different, indicating that in addition to chordwise oscillation, there are also spanwise fluctuation of shock wave.

The DMD mode contours and frequencies of AVERT wing are shown in Fig. 7 and Table. 1, respectively. The first-order mode is a static mode with zero frequency, which is close to the

## **INSERT RUNNING TITLE HERE**

averaged flow field. The frequency of second-order mode is f=78. 85Hz, which is basically consistent with the peak frequency of the pressure spectrum. The mode contours show that the second-order mode characterizes the spanwise fluctuation of shock wave. The frequency of the third-order mode (152.02Hz) is about twice that of the second-order mode. Therefore, the second-order mode is the global mode that dominates the shock buffet flow characteristics in this state. Unlike wing sections dominated by shock wave chordwise oscillation, shock buffet flow of swept wing is dominated by the spanwise fluctuation of shock wave.

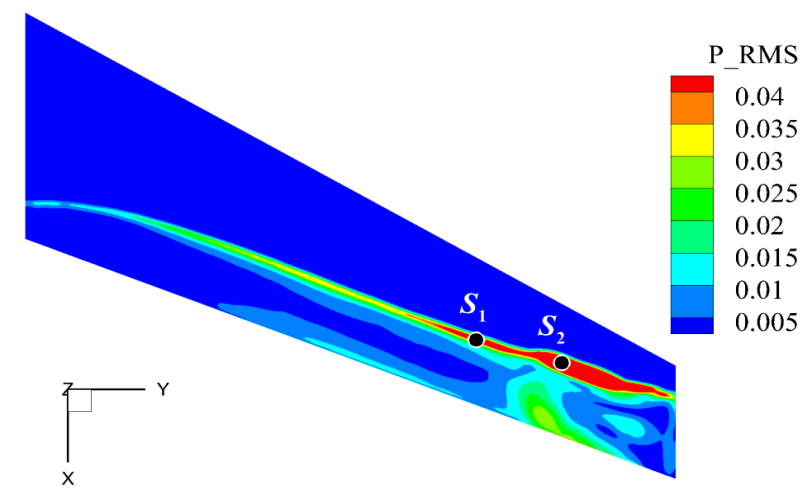


Figure 5 The RMS distribution of pressure on AVERT wing surface, Si is sampling point

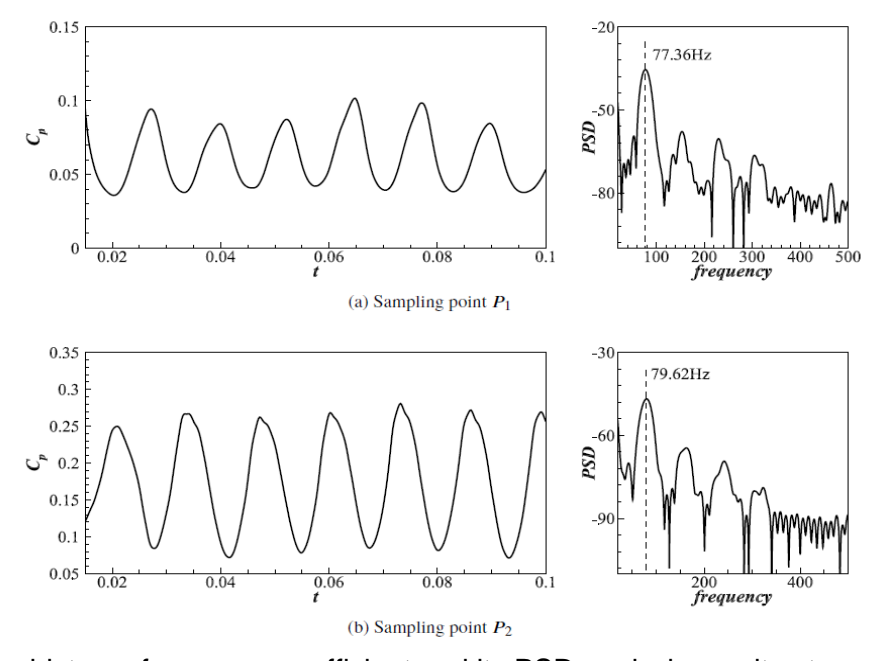


Figure 6 Time history of pressure coefficient and its PSD analysis results at sampling points.

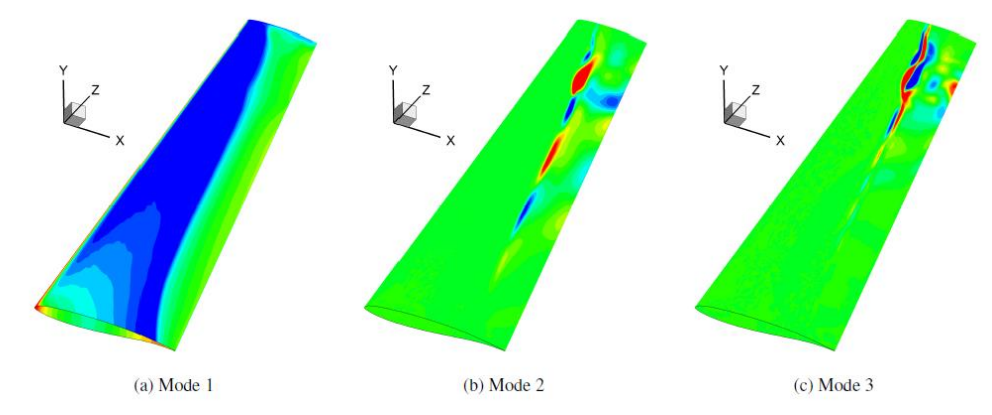


Figure 7 First 3 DMD mode contours of shock buffet flow for AVERT wing.

Table 1 First 3 DMD mode frequencies of shock buffet flow for AVERT wing

Mode	1	2	3
Physical frequency	0Hz	78.85 <i>Hz</i>	152.02 <i>Hz</i>
Reduced frequency	0	0.35	0.67

# 4.2 Control of the Shock Buffet Flow Control for AVERT Wing

For the shock buffet flow of AVERT wing dominated by spanwise fluctuation of shock wave, this study also uses the active-passive cooperative control scheme, and the control mechanism is shown in Fig. 8. The individual control scheme and its control results will be introduced first, and then compared with the results of the active-passive cooperative control scheme.

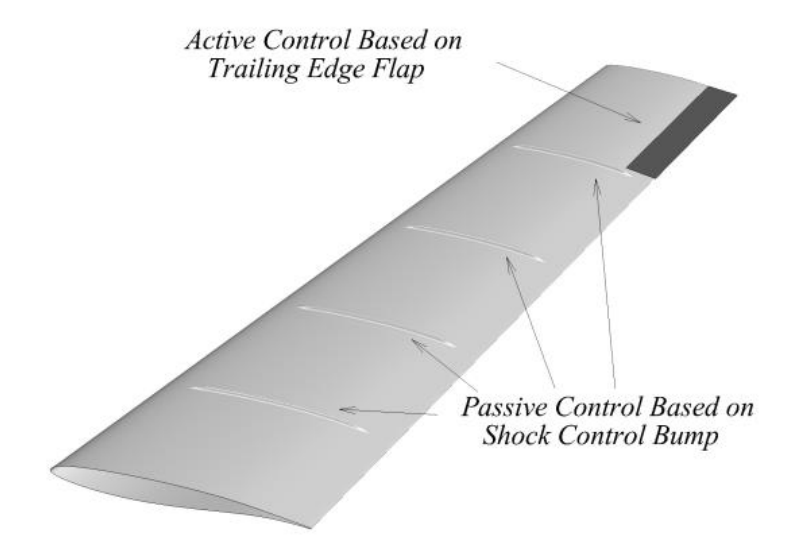


Figure 8 Schematic diagram of the trailing edge flap and shock control bump on AVERT wing The active control scheme is the same as that designed for the wing section with an aspect ratio of 0.25 mentioned above. The feedback signal is still the lift coefficient Cl. The actuator is a 15% chord length flap surface at the trailing edge. Due to significant pressure pulsation near the wing tip, the spanwise range of the flap surface is 0 to 0.2L from the end surface of wing tip, as shown in Fig. 8, and the control signal is the flap deflection angle β. The feedback control law obtained by model-free adaptive control (MFAC) method. The time history of lift coefficient and flap deflection angle during the control process is shown in Fig. 9. Similar to the active control result of the wing section with an aspect ratio of 1.0, due to the significant impact of shock wave spanwise fluctuation, using only the trailing edge flap cannot completely eliminate shock wave fluctuation and the resulting lift fluctuation. It can only reduce the amplitude of the lift coefficient fluctuation from 0.009 to 0.003, and the flap deflection angle still needs to be continuously deflected. The comparison of pressure RMS on the surface of the AVERT wing before and after the active control is turned on. It can be seen that the pressure pulsation has almost not weakened, indicating that the decrease in the lift coefficient is caused by the offset of flap deflection and shock wave oscillation. So, the active control system has not successfully eliminated the shock buffet of AVERT wing.

The control effect with only the passive manner is also investigated. The role of SCB is analyzed, and the arrangement scheme of SCB as shown in Fig.8 is adopted. The height variation of the SCB along the chordwise and spanwise directions is a Hicks Henne shape function. In chordwise direction, the starting position of the bump is taken as  $x_0 = 0.1c_y$ , and the length is  $l_{bx} = 0.8c_y$ , where  $c^y$  is the local chord length. In spanwise direction, the crest locations of four bumps are 0.4L, 0.6L and 0.8L, the length of the bump  $l_{by}$  is 0.005L. The shape of the bump is symmetric, and the height of the bump  $h_b = 0.01c_y$ , where c is mean aerodynamic chord length. For the passive control of shock buffet, the comparison of lift coefficient between the above AVERT wing with SCB and the clean AVERT wing

is shown in Fig. 10. Compared with the clean AVERT wing, the lift coefficient fluctuation amplitude of the AVERT wing with SCB does not decrease, but the fluctuation frequency is significantly reduced. The RMS distribution of pressure on the surface of AVERT wing with SCB is shown in Fig. 11 (c). Compared with clean wing section (Fig. 11 (a)), the amplitude of pressure pulsation does not significantly decrease, but the range of shock wave oscillation changes, resulting in changes in the areas with larger pressure pulsation.

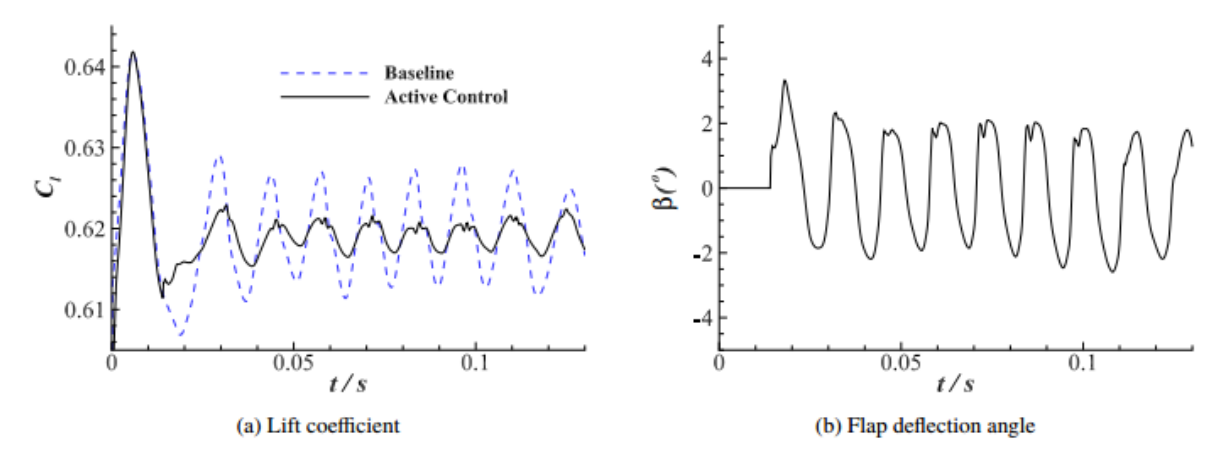


Figure 9 Time history of the lift coefficient and flap deflection angle with only active control of flap

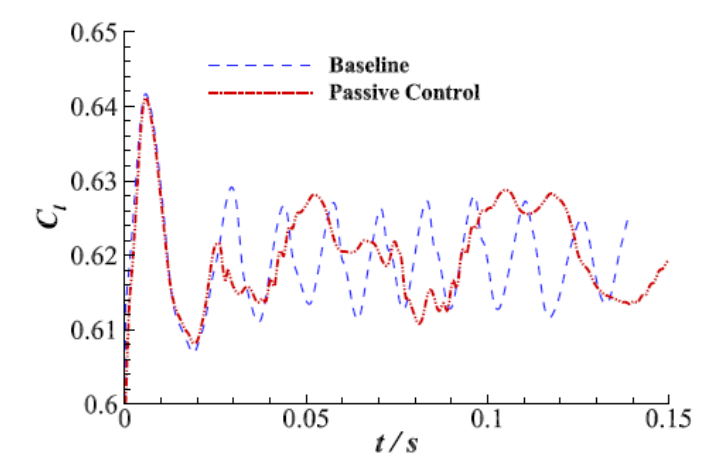
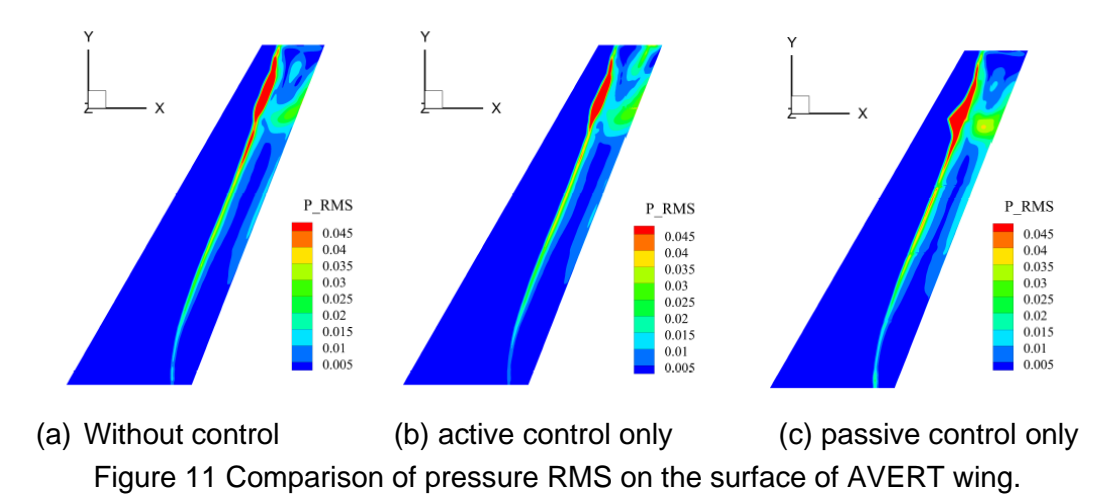


Figure 10 Comparison of lift coefficient time history between the AVERT wing with SCB (passive control) and the clean AVERT wing (baseline).



Based on above control results, this study adopts the active-passive cooperative control scheme to simultaneously suppress the spanwise fluctuation and chordwise oscillation of shock wave. The time histories of lift coefficient, drag coefficient, and flap deflection angle during the control process are shown in Fig. 12. It can be seen that after the APCC is turned on, the lift fluctuation basically

#### **INSERT RUNNING TITLE HERE**

disappears, and the time-averaged lift coefficient increases from 0.6192 before the control to 0.6278 after the control. The fluctuation amplitude of the drag coefficient decreases from 7.0×10<sup>-4</sup> to 2.0×10<sup>-4</sup>, with the time-averaged value changing from 4.75×10<sup>-2</sup> to 4.77×10<sup>-2</sup>. The final deflection amplitude of the control surface is approximately 0.3 deg.. The comparison of pressure RMS before and after control is shown in Fig.13, it can be seen that the pressure pulsation is significantly reduced. The pressure RMS at the cross-section with the largest pressure pulsation. Aside from observing a decrease in the amplitude of pressure pulsation and a reduction in the region of shock wave oscillation, it can also be noticed that the use of SCB has a similar effect to that of a wing fence. It can restrict spanwise flow in the boundary layer, alleviate the flow separation at the wing tip, and slightly shift the position of shock wave downstream, which is the reason for the increase in lift coefficient.

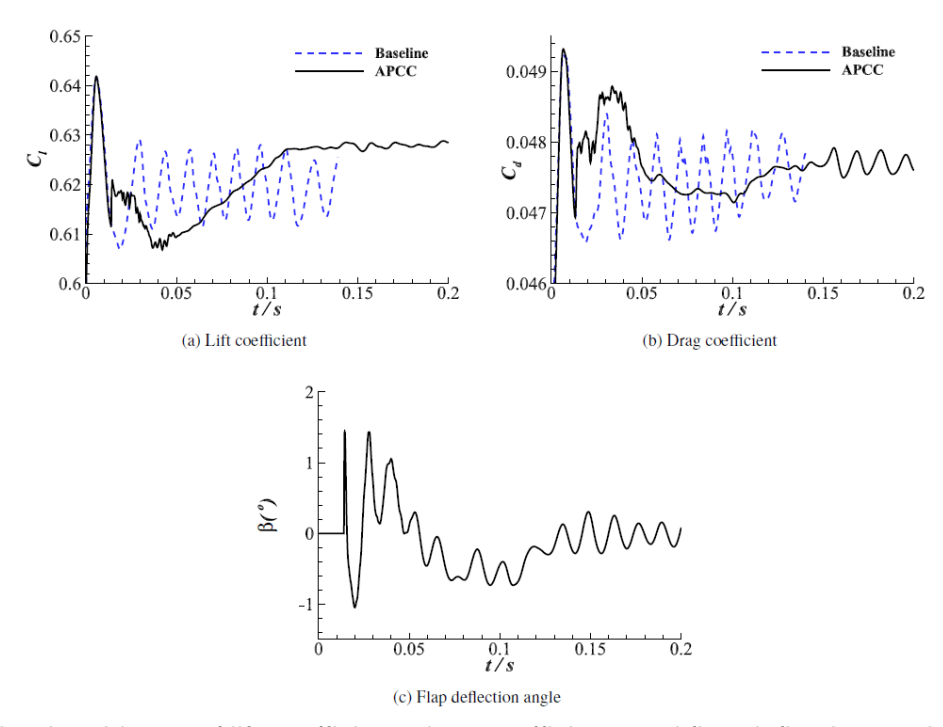


Figure 12 The time history of lift coefficient, drag coefficient, and flap deflection angle of AVERT wing during the APCC process.

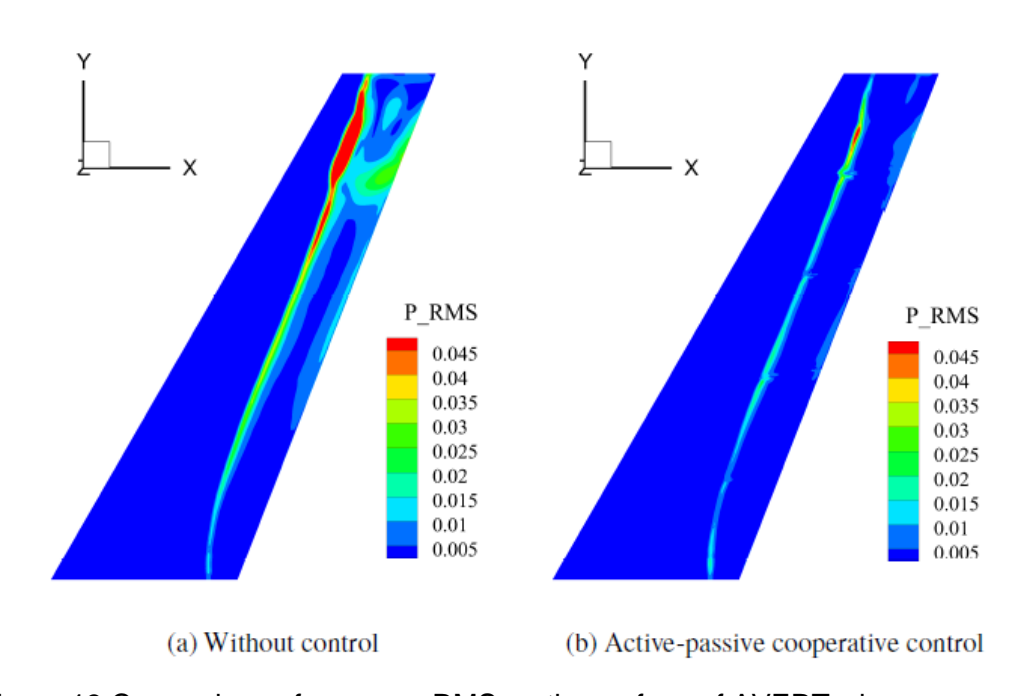


Figure 13 Comparison of pressure RMS on the surface of AVERT wing.

## **Copyright Statement**

The authors confirm that they, and/or their company or organization, hold copyright on all of the original material included in this paper. The authors also confirm that they have obtained permission, from the copyright holder of any third party material included in this paper, to publish it as part of their paper. The authors confirm that they give permission, or have obtained permission from the copyright holder of this paper, for the publication and distribution of this paper as part of the ICAS proceedings or as individual off-prints from the proceedings.

### References

- [1] Giannelis, N. F., Vio, G. A., and Levinski, O., "A review of recent developments in the understanding of transonic shock buffet," Progress in Aerospace Sciences, Vol. 92, 2017, pp. 39–84.
- [2] Gao, C., and Zhang, W., "Transonic aeroelasticity: A new perspective from the fluid mode," Progress in Aerospace Sciences, Vol. 113, 2020, p. 100596.
- [3] Masini, L., Timme, S., and Peace, A., "Analysis of a civil aircraft wing transonic shock buffet experiment," Journal of Fluid Mechanics, Vol. 884, 2020, p. A1.
- [4] [Gao, C., and Zhang, W., "Numerical simulation and modal analysis of transonic buffet flow over wings," Acta Aeronautica Astronautica Sinica, Vol. 40, No. 7, 2019, pp. 122597–122597.
- [5] Jacquin, L., Molton, P., Deck, S., Maury, B., and Soulevant, D., "Experimental study of shock oscillation over a transonic supercritical profile," AIAA journal, Vol. 47, No. 9, 2009, pp. 1985–1994.
- [6] Roos, F., "The buffeting pressure field of a high-aspect-ratio swept wing," 18th Fluid Dynamics and Plasma dynamics and Lasers Conference, 1985, p. 1609.
- [7] Yun, T., Shiqi, G., Peiqing, L., and Jinjun, W., "Transonic buffet control research with two types of shock control bump based on RAE2822 airfoil," Chinese Journal of Aeronautics, Vol. 30, No. 5, 2017, pp. 1681–1696.
- [8] Smith, A., Babinsky, H., Fulker, J., and Ashill, P., "Shock wave/boundary-layer interaction control using streamwise slots in transonic flows," Journal of Aircraft, Vol. 41, No. 3, 2004, pp. 540–546.
- [9] Huang, J., Xiao, Z., Liu, J., and Fu, S., "Simulation of shock wave buffet and its suppression on an OAT15A supercritical airfoil by IDDES," Science China Physics, Mechanics and Astronomy, Vol. 55, 2012, pp. 260–271.
- [10]Sidorenko, A., Budovsky, A., Polivanov, P., Vishnyakov, O., Sudakov, V., and Ishchenko, V., "Suppression of transonic buffet with plasma vortex generators," Thermophysics and Aeromechanics, Vol. 26, 2019, pp. 465–480.
- [11]Gao, C., Zhang, W., Kou, J., Liu, Y., and Ye, Z., "Active control of transonic buffet flow," Journal of Fluid Mechanics, Vol. 824, 2017, pp. 312–351.
- [12]Petrocchi, A., Mauriello, M., and Barakos, G., "Transonic Buffet Alleviation via Virtual Control Surfaces," Aerospace Science and Technology, 2023, p. 108478.
- [13]Mayer, R., Lutz, T., and Krämer, E., "Numerical study on the ability of shock control bumps for buffet control," AIAA Journal, Vol. 56, No. 5, 2018, pp. 1978–1987.
- [14]Mayer, R., Lutz, T., Krämer, E., and Dandois, J., "Control of transonic buffet by shock control bumps on wing-body configuration," Journal of Aircraft, Vol. 56, No. 2, 2019, pp. 556–568.
- [15]Molton, P., Dandois, J., Lepage, A., Brunet, V., and Bur, R., "Control of buffet phenomenon on a transonic swept wing," AIAA Journal, Vol. 51, No. 4, 2013, pp. 761–772.
- [16]Dandois, J., Lepage, A., Dor, J.-B., Molton, P., Ternoy, F., Geeraert, A., Brunet, V., and Coustols, É., "Open and closed-loopcontrol of transonic buffet on 3D turbulent wings using fluidic devices," Comptes Rendus Mécanique, Vol. 342, No. 6-7, 2014, pp. 425–436.
- [17]Levy, D., Laflin, K., Vassberg, J., Tinoco, E., Mani, M., Rider, B., Brodersen, O., Crippa, S., Rumsey, C., Wahls, R., et al., "Summary of data from the fifth AIAA CFD drag prediction workshop," 51st AIAA Aerospace Sciences Meeting including the New Horizons Forum and Aerospace Exposition, 2013, p. 46.
- [18]Ohmichi, Y., Ishida, T., and Hashimoto, A., "Numerical investigation of transonic buffet on a three-dimensional wing using incremental mode decomposition," 55th AIAA Aerospace Sciences Meeting, 2017, p. 1436.
- [19]Koike, S., Ueno, M., Nakakita, K., and Hashimoto, A., "Unsteady pressure measurement of transonic buffet on NASA common research model," 34th AIAA applied aerodynamics conference, 2016, p. 4044.
- [20]Dandois, J., "Experimental study of transonic buffet phenomenon on a 3D swept wing," Physics of Fluids, Vol. 28, No. 1, 2016.